Neuroimage: Reports 6 (2026) 100305

Contents lists available at ScienceDirect

Neuroimage: Reports

journal homepage: www.sciencedirect.com/journal/neuroimage-reports

The relation between neuroinflammation, amyloid-β load, grey matter loss and brain activity in visual object recognition regions in Alzheimer's Disease

Lília Jorge [a,b,d], Nádia Canário [a,b,c], Ricardo Martins [a,b], Antero Abrunhosa [a,b], Isabel Santana [e], Miguel Castelo-Branco [a,b,c,*]

[a] Coimbra Institute for Biomedical Imaging and Translational Research (CIBIT), University of Coimbra, Portugal
[b] Institute for Nuclear Sciences Applied to Health (ICNAS), University of Coimbra, Portugal
[c] Institute of Physiology, Faculty of Medicine (FMUC), University of Coimbra, Portugal
[d] Faculty of Sciences and Technology (FCTUC), Department of Physics, University of Coimbra, Portugal
[e] Coimbra University Hospital Centre (CHUC), Department of Neurology, Portugal

ARTICLE INFO

Keywords:
Alzheimer's disease
Amyloid-β
Neuroinflammation
Cortical atrophy
Functional activity
Visual ventral stream regions

ABSTRACT

The regional impact of amyloid-β (Aβ) load and neuroinflammation on brain integrity and function is essential to understand the pathophysiology of Alzheimer's disease (AD), yet it is still lacking in the current literature, particularly in regions involved in visual object recognition.

Here, using a multimodal approach, we investigated AD-related neuropathological changes and their impact on task-related responses in core visual object recognition areas of the ventral stream: FFA, FBA, LOCv, PPA and VWFA. We combined 11C-PK11195 PET measures of neuroinflammation, 11C-PIB PET measures of Aβ load, MRI structural measures of grey matter and functional MRI (fMRI) BOLD response, using a visual recognition task, in 20 AD patients and 17 Aβ negative healthy controls. Mixed repeated-measure ANOVAS were computed to assess which regions differed between groups for each data modality, and partial correlation tests were used to explore associations across modalities.

We found in mild AD patients higher levels of atrophy and Aβ, as compared to relatively preserved visual activation and neuroinflammation levels. An association between Aβ levels and neuronal response was found in right LOCv, possibly suggesting an early transient subclinical impact of Aβ on brain function. We also found an interesting pattern of hemispheric asymmetry, with concurrent atrophy and Aβ load in the left hemisphere.

Overall, these findings suggest differential vulnerability to pathological processes along the visual ventral stream in AD, characterized by relatively preserved functional response and neuroinflammatory status, alongside increased leftward susceptibility to GM atrophy and Aβ deposition.

1. Introduction

Alzheimer's disease (AD) is a progressive neurodegenerative disorder characterized by distinct stages of severity based on the level of cognitive impairment (American Psychiatric Association, 2000). Its neuropathological hallmarks comprise abnormal amyloid-β (Aβ) deposition, neurofibrillary tangles (NFTs), cortical atrophy, neuroinflammation and subsequent cognitive decline (Avila et al., 2016; Bloom, 2014; Hardy and Selkoe, 2002; Pasqualetti et al., 2015; Selkoe, 2004). It is now accepted that these features do not appear simultaneously but rather with distinct temporal patterns and with a significant lag between them (Jack et al., 2010; Jagust, 2018; Villemagne et al., 2013). According to Jack et al. (2010), abnormal Aβ deposits emerge initially, possibly reaching a plateau before neurodegeneration and clinical symptoms become apparent. In turn, grey matter (GM) loss manifests later in the natural history of AD, albeit still at the pre-symptomatic stage, before cognitive impairment becomes overt. This temporal ordering of abnormalities and their progressive spreading throughout specific networks of the brain (Kuczynski et al., 2010; Lo et al., 2010; Raj et al., 2012) imply that, at a certain time point

* Corresponding author. Coimbra Institute for Biomedical Imaging and Translational Research (CIBIT), University of Coimbra, Azinhaga de Santa Comba, 3000-548, Coimbra, Portugal.
E-mail address: mcbranco@fmed.uc.pt (M. Castelo-Branco).

https://doi.org/10.1016/j.ynirp.2025.100305
Received 24 August 2025; Received in revised form 29 November 2025; Accepted 2 December 2025
Available online 8 December 2025

different brain regions may be undergoing different neuropathological processes, i.e., at the same time point some regions might be under an Aβ loading phase, others in an early neuronal dysfunction phase, whereas others might be already in a cognitive dysfunction phase (Jack et al., 2010).

At early stages, the temporal cortex and the hippocampus appear predominantly affected, leading to memory loss (Baudic et al., 2006; Marshall et al., 2011), while other cognitive abilities, such as visual recognition, remain relatively preserved (Done and Hajilou, 2005; Ferman et al., 2006; Mendez et al., 2002). Multiple processing streams are known to be involved in visual function (Sereno et al., 1995; Tyler et al., 2005; Wandell et al., 2005), with dorsal and ventral stream regions differentially dedicated to vision for action and recognition processes, respectively (Haxby et al., 1991; Pihlajamäki et al., 2005). In particular, the ventral pathway accounts for conscious visual perception of objects, faces, and colours (Mishkin et al., 1983). It includes several visual regions such as, the fusiform face area (FFA) which is involved in face recognition, the fusiform body area (FBA) in body image processing, the ventral part of the lateral occipital cortex (LOCv) in object recognition, the parahippocampal place area (PPA) in scene recognition and the visual word form area (VWFA) in processing of verbal material (Canário et al., 2016; Cichy et al., 2011; Downing and Peelen, 2011; Grill-Spector et al., 2001, 2004; Jorge et al., 2018; Liu et al., 2008). These higher-order visual regions are located in the inferior temporal lobe, and their involvement in AD remains an open question. Nevertheless, the studies by Graewe et al. (2013) and Sauer et al. (2006) are notable exceptions, suggesting impaired responses in FFA and superior temporal sulcus (STS) using fMRI tasks in mild cognitive impairment (MCI) and mild AD patients, respectively. Moreover, we found previously that among a broad set of visual areas, only the right FBA and VWFA showed minimal functional alterations in mild AD (Canário et al., 2023). However, multimodal studies addressing the neuropathological alterations of these specific brain regions and their impact on brain function are notably lacking in AD, other than resting state studies. In a previous study, we investigated these associations in the posterior cingulate cortex (PCC), focusing on the memory/executive component of the fMRI task (Canário et al., 2022). Here, we extend this approach to the visual ventral recognition regions for the first time. A few studies have explored multimodal associations with resting state fMRI outcomes in other brain regions (Hrybouski et al., 2024; Thompson et al., 2024; Zheng et al., 2019).

Whole-brain studies in mild AD have provided evidence of substantial cortical atrophy, expressive Aβ burden (Jorge et al., 2021), and NFTs (Braak and Braak, 1991) across multiple brain regions, including inferotemporal cortex, whereas results pertaining to neuroinflammation are quite inconsistent (Cagnin et al., 2001; Fan et al., 2017; Hamelin et al., 2016; Wiley et al., 2009; Yokokura et al., 2011). Surprisingly, despite evidence of such neuropathological burden, these visual areas appear to largely maintain their function in the early stages of the disease (Canário et al., 2023), which is compatible with the early clinical amnestic presentation of the disease. As such, focusing on less functionally damaged regions, where the mechanisms accounting for the AD pathophysiology are not fully established, and linking different processes, including fMRI task-related activity, may help to disentangle the complex relationship between neuropathological markers, the processes they reflect, and cognitive function. Therefore, the goal of the present study was to scrutinize group differences in Aβ deposition, neuroinflammation, and neurodegeneration and their impact on neuronal activity in FFA, FBA, PPA, LOCv, and VWFA visual regions in the AD group. For that, we undertook a multimodal neuroimaging study to combine GM density as an index of cortical atrophy, 11C-PK11195 quantification of neuroinflammation, 11C-PiB SUVR quantification of cerebral Aβ and fMRI to study task-related neural activation assessed by means of BOLD (blood oxygenation level dependent) response in mild AD, and a matched control group.

As far as we know, this is the first multimodal study to evaluate the regional coupling between functional responsiveness as measured by task-related functional BOLD fMRI and AD classical neuroimaging markers indexing brain pathology, particularly in visual ventral regions. Focusing our efforts on specific regions in which both neuropathological measures and neuronal function are available is extremely important and a unique opportunity to link pathophysiological features to brain function.

Based on the lack of multimodal evidence on impairments in visual recognition areas, we asked whether a high neuropathological burden can occur in the visual ventral stream regions despite a relatively preserved visual functional response.

2. Methods

2.1. Participants

Overall, we enrolled in this study 41 individuals of whom 20 were patients with clinical diagnosis of probable AD, supported by biological biomarkers (cerebrospinal fluid (CSF) and/or 11C-PiB PET) from the Memory Clinic of the Centro Hospitalar e Universitário de Coimbra (CHUC), and 21 were healthy controls (HC) matched for age, sex, and education. Some of the participants included in the current study were also part of a previously published dataset (Canário et al., 2023).

All AD patients were at a mild stage of dementia in line with the Clinical Dementia Rating (CDR = 1). The clinical diagnosis was made by two trained neurologists following the tenets of Diagnostic and Statistical Manual of Mental Disorders – fourth edition (DSM-IV-TR) (American Psychiatric Association, 2000) and the National Institute of Neurological and Communicative Disorders and Stroke- Alzheimer's Disease and Related Disorders (NINCDS-ADRDA) (McKhann et al., 2011). Finally, CSF biomarkers cut-offs applied in this study were as follows: 580 pg/mL for Aβ1–42, 0.068 for Aβ42/Aβ40, 250 pg/mL for Tau, and 37 pg/mL for pTau. Regarding the 11C-PiB PET imaging, the Aβ positivity was determined by a visual assessment conducted by an experienced nuclear medicine physician. In this approach, for each PET 11C-PiB image, a fixed colour scale with an upper SUVR limit of 2.5 was defined to standardize interpretation. The images were evaluated with a focus on the frontal, parietal/precuneus, temporal, anterior and posterior cingulate, basal ganglia, and occipital cortices. More information about the clinical characterization of the AD group can be found in previous works (Canário et al., 2022; Jorge et al., 2021).

The HC group comprised 21 healthy volunteers absent of neurologic or psychiatric disorders. The normal cognitive status of this group was assured by a brief cognitive assessment. Hence, all HC exhibited no significant memory complaints (Subjective Memory Complaints Questionnaire - SMC $\leq$3) (Ginó et al., 2008; Schmand et al., 1996), normal general cognitive function as measured by the MoCA (mean $\pm$ standard deviation (SD) = 24.88 $\pm$ 4.24) (Freitas et al., 2011), maintained daily living activities (Lawton & Brody scale – L&B: for female = 8; for male = 5) (Barreto et al., 2008; Lawton and Brody, 1969; Madureira, S. & Verdelho, 2008; Yesavage et al., 1983) and no moderate or severe depressive symptoms (30-item Geriatric Depressive Scale – GDS = 30, mean $\pm$ SD, 6.41 $\pm$ 6.20). All participants underwent MRI and fMRI acquisition in the same scanning session, while 11C-PiB PET and 11C-PK11195 PET scans were performed on separate days. The interval between MRI and PET acquisitions did not exceed 5 weeks in AD cases.

This work followed guidelines and regulations approved by the Ethics Committee of the University of Coimbra, according to the Declaration of Helsinki, and all participants gave their informed written consent for the study.

2.2. MRI and fMRI imaging pre-processing

Data from magnetic resonance imaging were collected using a Siemens Magnetom TIM Trio 3 T scanner (Siemens, Munich, Germany) with a phased array 12-channel birdcage head coil. The structural data

consisted of 3D structural MR imaging scans using a T1-weighted MPRAGE (magnetization-prepared rapid gradient echo) magnetic resonance imaging pulse sequence, with the following settings: TR = 2530 ms, TE = 3.42 ms, TI = 1100 ms, flip angle 7°, 176 single-shot interleaved slices with no gap, isotropic voxel size 1 × 1 × 1 mm; FOV 256 mm. Data from the two functional runs were acquired using the following parameters: TR = 2000 ms, TE = 30 ms, voxel size = 2.5 × 2.5 × 3 mm, FOV = 256 × 256 mm, matrix size = 102 × 102, and a flip angle of 90°. In each functional run, 31 slices and a total of 276 vol were acquired.

To assess brain structural integrity, the anatomic sequences were processed in MATLAB software (version 8.1.0 $R^{20}13a$, The Mathworks, MA) using the computational anatomy toolbox (CAT12) (http://dbm.neuro.uni-jena.de/cat/) of the SPM12 (Version 12, Wellcome Trust Centre for Neuroimaging, London, UK) and employing the VBM (voxel-based morphometry) method. VBM provides the voxel-wise estimation of the GM density, which we used as an index of atrophy. CAT12 allows fully automatic cortex segmentation and has a pipeline which we follow mostly with the default settings: T1-weighted images were normalized to a template space and automatically segmented into GM, white matter (WM), and CSF. The automatic segmentation relies on prior probability tissue maps and assigns to each voxel a value representing the proportion of the corresponding tissue type (GM, WM and CSF) (Ashburner and Friston, 2005). Then, resorting to the high-dimensional registration DARTEL algorithm (Ashburner, 2007), which uses linear affine transformation followed by non-linear warping, the spatial normalization was performed, aligning subject's brain to a standard MNI template. Thereafter, Jacobian modulation was applied (Ashburner and Friston, 2000) to restore tissue volumes that were altered during the normalization processing. Afterwards, the normalized GM images were smoothed using an 8-mm FWHM kernel to improve accuracy of anatomical standardization. The resulting values were therefore used as an index of brain structural integrity.

The procedure regarding the functional dataset is detailed in our previous study (Canário et al., 2023). Briefly, the anatomical images used for coregistration underwent correction for signal intensity inhomogeneity, reorientation to the AC-PC plane, and transformation into the Talairach reference system (TAL). The raw fMRI images were submitted to slice timing correction, temporal filtering, as well as corrections for signal intensity and motion. Subsequently, the pre-processed fMRI data in their native space were aligned with the anatomical scan, also in its native MRI space. The resulting image was subsequently converted to TAL space using the previously determined anatomical image transformation to the standardized space. The voxel size for the resampled fMRI data in TAL space was set to 1.0 × 1.0 × 1.0 mm. All the steps above are described in more detail elsewhere (Goebel et al., 2006). In total, six distinct categories of grey-scale visual stimuli were presented to all participants involved in the study: faces, bodies, objects, places, verbal material, and scrambled images. The experimental fMRI design consisted of two functional block design runs, during which the stimuli were presented randomly. Each run comprised 18 pseudo-randomized blocks with three blocks allocated to each stimulus category. Each block contained 20 images, each shown for about 800 ms with a 200 ms interval, totalizing 20 s per block. Blocks were separated by 10-s fixations with a uniform grey-scale image serving as the baseline. Participants performed a 1-back task, responding when consecutive images matched. An illustration of the fMRI task paradigm and examples of the visual categories used are provided in Supplementary Fig. 1.

2.3. PET acquisition, pre-processing and quantitative analysis

During the second and third visits, we acquired 11C-PiB PET and 11C-PK11195 PET scans using a Philips Gemini GXL PET/CT scanner (Philips Medical Systems, Best, the Netherlands). Each visit included a dynamic 3-dimensional PET scan of the entire brain (90 slices, 2-mm slice sampling) and a low-dose brain CT scan for attenuation correction. The 11C-PiB PET scan comprised 24 frames over 90 min (frame durations: 4 × 15s + 8 × 30s + 9 × 60s + 2 × 180s + 14 × 300s), while the 11C-PK11195 PET scan comprised 22 frames over 60 min (frame durations: 4 × 30s + 4 × 60s + 4 × 120s + 4 × 240s + 6 × 300s). We initiated image acquisition immediately after intravenous bolus injections of approximately 555 MBq of 11C-PiB or 370 MBq of 11C-PK11195, minimizing head movement by restraining participants' heads with soft elastic tape. The PET images were reconstructed into a 128 × 128 × 90 matrix with 2-mm isotropic voxel dimensions using the LOR RAMLA algorithm (Philips PET/CT Gemini GXL) with attenuation and scatter correction. Pre-processing and quantitative analysis were performed independently for both PET types. We obtained a sum image for each session by combining all dynamic PET frames. This sum image allowed us to estimate a rigid transformation between the PET image space and each participant's T1 anatomical MRI space, achieved through 3D Slicer 4.8.1 (www.slicer.org) (Kikinis et al., 2014). Individual MRI scans were spatially normalized to the Montreal Neurological Institute (MNI) template using the DARTEL algorithm (Ashburner, 2007) in SPM12.

Voxel-level quantitative analysis of 11C-PiB PET and 11C-PK11195 PET images was conducted in MNI space using in-house custom software. For 11C-PiB PET, we computed individual standard uptake value ratio (SUVR) maps by summing voxel-level signal from 40 to 70 min post-injection and dividing by the mean signal from the cerebellar grey matter (excluding the cerebellar peduncles) as the reference region (Bonilla and Carril, 2013; McNamee et al., 2009; Oliveira et al., 2018). For 11C-PK11195 PET, we generated individual Binding Potential (BP_{ND}) maps using the Multilinear Reference Tissue Model 2 (MRTM2) (Ichise et al., 2003). The reference region, identified by the SVCA4 algorithm (Supervised Cluster Analysis with 4 classes: grey matter without specific binding, white matter, blood, grey matter with specific binding) (Yaqub et al., 2012), comprised grey matter voxels exhibiting kinetic activity similar to normal grey matter without 11C-PK11195 specific binding. We resampled PET SUVR and BP_{ND} maps to the anatomical image space to ensure consistent dimensions. Prior to conducting the SPM12 analysis, the PET SUVR and BP_{ND} maps were smoothed with an 8x8x8 mm FWHM Gaussian filter.

3. Statistical analysis

In our initial approach, we chose to exclude 4 HC participants who were Aβ positive, to avoid including preclinical AD patients, resulting in a sample of 20 AD and 17 HC participants. For the 11C-PK11195 PET BP_{ND}19 AD patients were considered given that one patient gave up the PET exam, while for the fMRI analysis 19 AD and 16 HC were considered, as data from two participants were excluded due to poor fMRI acquisition quality. Subsequently, we conducted a sensitivity analysis that included 3 Aβ-positive HC participants with available data.

The Shapiro-Wilk test was firstly used to assess the distribution of both neuropsychological, demographic, and behavioural data and then the unpaired T-test or its non-parametric version - the Mann-Whitney test were accordingly used for the between-groups comparisons. Comparisons between categorical variables (sex) were in turn examined with Fisher's Exact Test.

We first identified 5 distinct areas from the ventral visual stream - FFA, FBA, LOCv, PPA, and VWFA, by computing a multi-subject random-effect general linear model (RFX-GLM) analysis, as implemented on Brainvoyager QX 2.8.2 (BrainInnovation, Maastricht, the Netherlands) software, and the procedure is detailed in our previous study (Canário et al., 2023). Briefly, each region of interest (ROI) was identified using specific contrasts set to highlight the functional attributes of each region, and all were used in previous papers (Canário et al., 2016, 2023; Jorge et al., 2018). Thus, for the FFA we used the conjunction contrast [faces > places] AND [faces > scrambled] AND [faces > objects], for the FBA we used [bodies > objects], for the LOCv we used [bodies > scrambled], and for the VWFA we selected [verbal >

scrambled]. We have also used a conjunction contrast to identify the PPA – [places > faces] AND [places > objects]. Given some heterogeneity in detecting each ROI, statistical thresholds for each t-maps were independently defined to localize each ROI, being that the least conservative threshold set on 0.01 uncorrected. All regions were functionally identified in both hemispheres, with the exception of the right VMFA for which we used the principle of homotopy to define a mirror ROI (Davies-Thompson et al., 2016), given the well-known functional laterality of this region. The delineated ROIs are shown in Fig. 1.

The estimated effects (beta values) of the preferred category stimuli were subsequently extracted for each ROI at an individual level, i.e. – FFA (face stimulus), FBA (bodies images), PPA (place stimulus), and VWFA (images of words). Each value extracted for the estimated effect was corrected for serial correlations. These values were then used as indexes of neuronal activity related to the visual function of each area. Thereafter, we used these functional ROIs to obtain the ROI mean values regarding the other data modalities: 11C-PiB SUVR, GM density, and 11C-PK11195 BP_{ND}. For that, the ROIS extracted from fMRI data in the TAL space were converted to the MNI space using GingerALE software (http://brainmap. org/ale/). Then, we used an in-house MATLAB SPM script that determined the arithmetic mean of the 11C-PiB SUVR, GM density, and 11C-PK11195 BP_{ND} maps within each ROI.

We further computed for each data modality – GM density, 11C-PiB-SUVR, 11C-PK11195 BP_{ND}, and beta values related to functional data – a Three-Way mix ANOVA repeated measure – using 2 Within-Subjects factors – ROI (5 levels: FBA, FFA, LOCv, PPA and VWFA) and hemisphere (2 levels: right and left) and Group as a Between-Subjects factor. Additional post-hoc pairwise comparisons with Bonferroni correction were performed for Within-Subjects main effects and interactions identified in the first analysis level. A one-way ANOVA with planned contrasts (independent sample t-tests) was used to examine the subsequent main effect of group.

The required assumptions of the mixed repeated measures ANOVA were firstly assessed, namely the normal distribution of all dependent variables across both groups with Shapiro-Wilk. The matrix sphericity was assessed with Mauchly test. Whenever the assumption of sphericity has not been met, we corrected the degrees of freedom of the F statistic by multiplying them by the Greenhouse-Geisser Epsilon factor. Additionally, to the between-subjects factor we have also been attentive to the required assumption of heteroscedasticity using the Levene's Statistic, assessed at all levels of our within-subjects variable.

Finally, partial correlations, controlling for age, were also performed between pathological markers and betas values to evaluate their impact on functional activity in the AD group. Finally, to test differences between mean total hemispheric values in the AD group we used a paired *t*-test. Statistical analyses were performed using IBM SPSS Statistics (version 27.0), and graphs were plotted using GraphPad Prism (version 6.0). The tests were performed two-tailed, and a probability of type I error (α) of 0.05 was considered. Adjustment for multiple comparisons were performed with Bonferroni method.

4. Results

Results regarding the demographic and clinical data are displayed in Table 1. A significant difference, as expected, was found regarding MoCA scores while no significant differences in age, sex, or education were found between groups.

Results of the behavioural data are provided in Supplementary material.

4.1. Results from mixed repeated-measures ANOVA to the GM data

GM density estimated means and SD to all five ROIs and for both hemispheres to the AD and CT groups are illustrated in Fig. 2. ANOVA statistics tests of Within-Subjects Effects have revealed a main effect of both predictors' ROI ($F(1.989, 69.607) = 57.406$, $p < 0.001$, $\eta_p^2 = 0.621$) and hemisphere ($F(1, 35) = 17.750$, $p < 0.001$, $\eta_p^2 = 0.336$) on GM values overall, suggesting that these values were different among ROIs and between hemispheres irrespective of group. In addition, a significant interaction between ROI x hemisphere was found ($F(1.563, 54.710) = 50.566$, $p < 0.001$, $\eta_p^2 = 0.591$), meaning that differences in GM density depend simultaneously on ROI and hemisphere when considering the two groups.

ANOVA statistics for the between-subjects tests revealed a significant main effect of group on the GM data ($F(1, 35) = 7.890$, $p = 0.008$, $\eta p2 = 0.184$). Planned contrasts between groups (AD < HC) showed significant differences (Bonferroni adjusted) in several regions: left FBA: $t(35) = 3.356$, p adjusted = 0.02, left FFA: $t(35) = 3.250$, p adjusted = 0.03, left VWFA: $t(35) = 3.409$, p adjusted = 0.02. A marginally significant effect was observed in the left PPA (p adjusted = 0.08). Other regions, including the right FBA, right FFA, left LOCv, and right VWFA, showed trends toward significance but did not survive correction.

Comparisons of total left and right hemispheric GM density revealed that values in the left hemisphere (mean GM: 0.423, SD: 0.060, N: 20) were significantly lower ($t(19) = -3.112$, $p = 0.006$) than on the right hemisphere (0.468, 0.087, 20), suggesting greater atrophy on the left side in the AD group.

Table 1
Demographic and neurophysiological sample characteristics.

	AD Group (n = 20) (mean ± SD)	HC Group (n = 17) (mean ± SD)	*p* value
Age	66.25 (6.87)	65.24 (7.00)	0.66
Female/male ratio	10/10	8/9	1.00
Education	9.30 (5.93)	11.59 (5.82)	0.26
MMSE	23.1 (2.97)	–	–
MoCA	14.26 (4.31)	24.94 (3.62)	<0.001*
CDR	1	–	–
ApoE-e4 (%)	95 %	–	–

Data are presented as mean (standard deviation); AD, Alzheimer's disease; HC, Healthy Controls; MMSE, Mini Mental State Examination; MoCA, Montreal Cognitive Assessment score; CDR, Clinical Dementia Rating. * Significant difference between the AD and HC group.

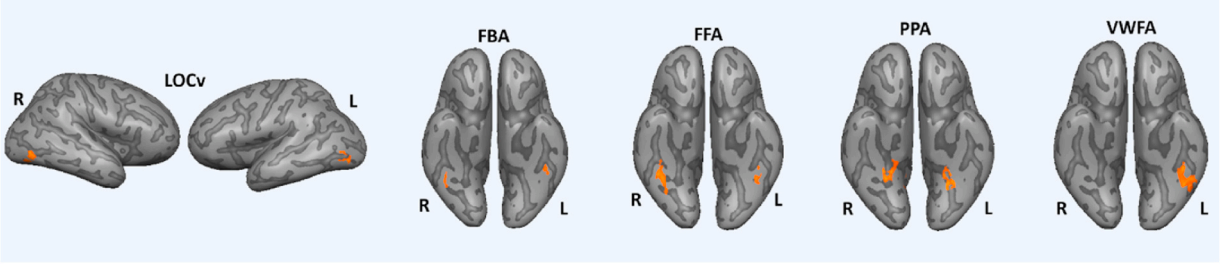

Fig. 1. Functionally defined LOCv, FBA, FFA, PPA, VWFA for right and left hemispheres using subject-specific volume time courses.

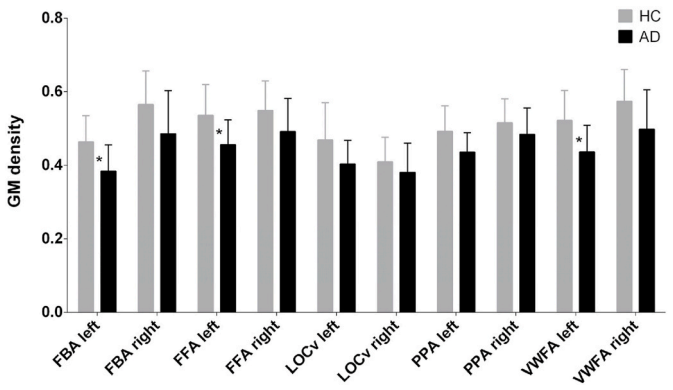

Fig. 2. Bar chart depicting the estimated mean and SD of GM density across all five ROIs and both hemispheres for the AD and HC groups. *Corrected for multiple comparisons with Bonferroni.

4.2. Results from mixed repeated-measures ANOVA regarding the Aβ data

Regarding the Aβ data, regional mean values for 11C-PiB SUVR uptake can be found in Fig. 3. ANOVA statistics tests of Within-Subjects Effects have revealed a significant main effect of both predictors' ROI ($F(2.097,73.394) = 44.966$, $p < 0.001$, $\eta_p^2 = 0.562$) and Hemisphere ($F(1, 35) = 6.737$, $p = 0.014$, $\eta_p^2 = 0.161$) on 11C-PiB uptake SUVR values overall, suggesting that the 11C-PiB uptake SUVR values were different for the ROIs as well as for both hemispheres. In addition, a significant interaction between ROI x hemisphere was found ($F(2.364, 82.745) = 3.161$, $p = 0.040$, $\eta_p^2 = 0.083$) as well as a significant interaction between ROI x Group ($F(2.097, 73.394) = 21.752$, $p < 0.001$, $\eta_p^2 = 0.383$), denoting differences in ROIs 11C-PiB uptake that depend on hemisphere and Group, respectively. Moreover, a triple interaction between ROI x Hemisphere x Group ($F(2.364, 82.745) = 8.833$, $p < 0.001$, $\eta_p^2 = 0.202$), suggesting that group differences were contingent on region and hemisphere. Post-hoc pairwise comparisons demonstrated that in the AD group, the left LOCv (mean SUVR: 1.716, SD: 0.065, N: 20) showed the highest Aβ levels, while the right PPA (1.321, 0.042, 20) had the lowest. These regional differences were statistically significant ($p < 0.001$).

ANOVA statistics for the between-subjects tests revealed a significant main effect of group on 11C-PiB-SUVR values overall ($F(1, 35) = 94.166$, $p < 0.001$, $\eta_p^2 = 0.729$). We also computed planned contrasts between groups (AD > HC) to check which ROIS were different. Results evidence significant differences bilaterally in FBA (right: $t(29.580) = 8.976$, $p < 0.001$, left: $t(26.327) = 8.561$, $p < 0.001$), FFA (right: $t(29.287) = 10.102$, $p < 0.001$, left: $t(27.974) = 9.401$, $p < 0.001$), LOCv (right: $t(24.276) = 7.776$, $p < 0.001$; left: $t(21.738) = 10.502$, $p < 0.001$), PPA (right: $t(26.604) = 6.628$, $p < 0.001$, left: $t(24.527) = 6.6990$, $p < 0.001$), VWFA (right: $t(28.492) = 10.207$, $p < 0.001$; left: $t(27.835) = 9.075$, $p < 0.001$). All these differences survived correction to multiple comparisons, as the Bonferroni-corrected p-value threshold = 0.005.

Moreover, in the AD group altogether the values of 11C-PiB SUVR on the left hemisphere (1.585, 0.22, 20) were significantly higher ($t(19) = 2.543$, $p = 0.020$) than on the right hemisphere (1.514, 0.20, 20), indicating a greater Aβ burden on the left side in the AD group.

4.3. Results from mixed repeated-measures ANOVA to the neuroinflammation data

Regional mean values for 11C-PK11945 BP_{ND} are depicted in Fig. 4. Tests of Within-Subjects Effects have revealed a significant main effect merely to the predictor ROI ($F(2.027, 68.910) = 25.159$, $p < 0.001$, $\eta_p^2 = 0.425$) on 11C-PK11945 BP_{ND} values overall. Considering both groups the values of 11C-PK11945 BP_{ND} were higher on the FBA (mean BP_{ND}: 0.414, SD: 0.018, N: 37), and VWFA (0.387, 0.017, 37), followed by LOCv (0.385, 0.023, 37), and FFA (0.362, 0.018, 37), and for last the PPA (0.239, 0.016, 37). No significant interactions emerged between factors. Likewise, ANOVA statistics for the between-subjects variable revealed no significant main effect of group on 11C-PK11195 BP_{ND} values overall ($F(1, 34) = 1.578$, $p = 0.218$, $\eta_p^2 = 0.044$).

4.4. Results from mixed repeated-measures ANOVA to the functional data

Estimated beta values concerning the functional dataset are depicted on Fig. 5. We obtained a main effect for ROI ($F(2.027,68.910) = 25.159$, $p < 0.001$, $\eta p^2 = 0.425$). Considering both groups, beta values were superior on the LOCv (mean beta: 0.958, SD: 0.088, N: 37), followed by FFA (0.844, 0.063, 37), PPA (0.666, 0.055, 37), FBA (0.539, 0.043, 37) and at last VWFA (0.257, 0.039, 37). In addition, a significant interaction between ROI x hemisphere was found ($F(3.534, 116.635) = 3.673$, $p = 0.010$, $\eta_p^2 = 0.10$), denoting differences in ROIs' beta values that depend on hemisphere. No more significant interactions were found between factors. The ANOVA statistics for the between-subjects tests revealed no significant main effect of group on beta values $F(1, 33) = 1.071$, $p = 0.308$, $\eta p^2 = 0.031$).

Results of all repeated-measures ANOVA remained virtually unchanged after including the 3 Aβ-positive HC participants. Detailed estimates from all sensitivity analyses are provided in the Supplementary Material.

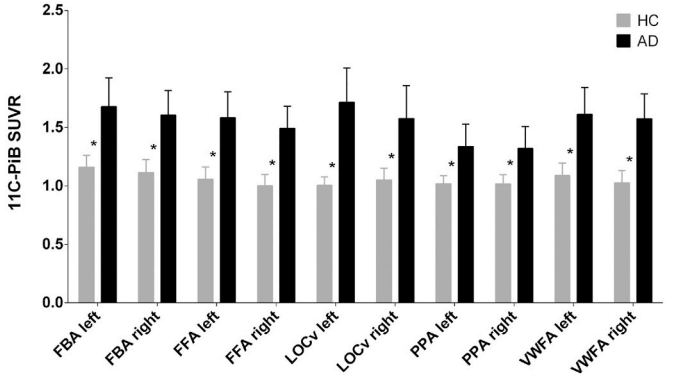

Fig. 3. Bar chart depicting the mean and SD of 11C-PiB SUVR uptake estimates across all five ROIs and both hemispheres for the AD and HC groups. *Corrected for multiple comparisons with Bonferroni.

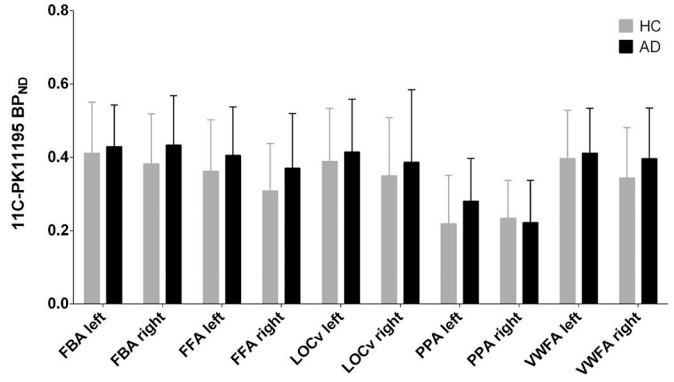

Fig. 4. Bar chart depicting the mean and SD of 11C-PK11195 BP_{ND} uptake estimates across all five ROIs and both hemispheres for the AD and HC groups. No statistically significant differences between groups were observed.

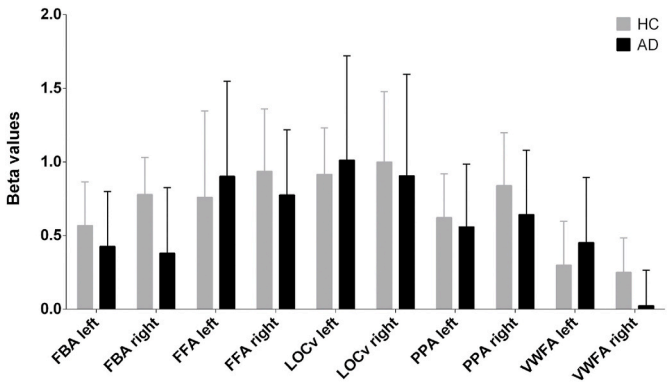

Fig. 5. Bar chart depicting the mean and SD of beta values across all five ROIs in both hemispheres for both the AD and HC groups. No statistically significant differences emerged between groups.

4.5. ROI-based correlation analysis

Partial correlation analyses were conducted for each functional ROI to examine associations between neuropathological markers (GM, Aβ and neuroinflammation) and functional activity. In the AD group, a significant correlation was observed only between fMRI activity (beta value) and 11C-PiB SUVR uptake in the right LOCv (r = - 0.674, p adjusted = 0.03, adjusted with Bonferroni for the total number of ROIs). The corresponding regression plots for both groups in this region are presented in Fig. 6. No significant correlations were found between modalities for the remaining ROIs. The results of all partial correlations computed are provided in Supplementary Table 1.

5. Discussion

This is the first study to investigate multimodal AD-related changes across five distinct visual ventral stream regions. Along with the investigation of the AD-related changes concerning functional response, structural integrity, Aβ load, and neuroinflammation status of the considered visual regions, the relationship between these cerebral measures was also investigated for the mild AD group.

Overall, we found group differences dependent on the hemisphere, region, and type of biological marker, offering novel insights into the AD-related damage of higher-order visual regions in a mild stage of the disease. Significant differences were found in visual ventral stream areas concerning GM density and Aβ deposition, but no significant differences

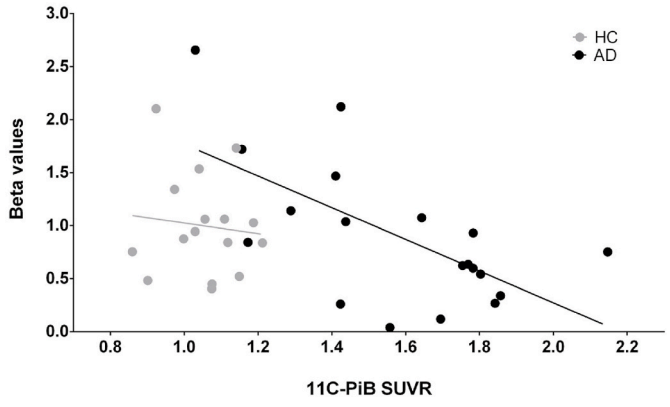

Fig. 6. Interplay between Aβ load and BOLD response in the right LOCv region to the AD and HC groups. A negative correlation emerged between Aβ load, quantified by the 11C-PiB SUVR, and the preferred stimulus beta value on the right LOCv for the AD group (r = - 0.674; p = 0.003) but not for the HC group (r = - 0.048, p = 0.864).

emerged in neuroinflammation levels and fMRI BOLD activation. In fact, at an early stage of AD, disproportionate changes in levels of NFT and Aβ levels in comparison to structural measures had been reported in the inferior temporal lobe (Braak and Braak, 1991; Jorge et al., 2021; Kreisl et al., 2013). In the present study, we found significant GM atrophy on the left-sided FBA, FFA and VWFA, whereas no significant differences emerged in left vLOC and right-sided homologues. This discrepancy between hemispheres atrophy perhaps suggests a time lag between the beginning of degeneration on both hemispheres, with the right starting later than the left, in line with the claimed asymmetric shrinkage of the brain in AD (Roe et al., 2021). Our findings are also in line with several studies reporting higher levels of atrophy in the left hemisphere compared to the right one (Chételat et al., 2002; Minkova et al., 2017; Whitwell, 2010). In contrast, the LOCv revealed no significant atrophy in either side, which might derive from its localization into the occipito-temporal sulcus, known to suffer from neurodegeneration later on (McDonald et al., 2009). Moreover, our results meet previous findings showing AD-related neuronal loss in distinct visual areas (Busatto et al., 2003, 2008; Matsuda, 2013; Whitwell, 2010) as well as in the inferior temporal lobe (Jorge et al., 2021). In particular, Busatto et al. (2003) reported a significant reduction of GM in the left fusiform/VWFA in both mild and moderate AD.

Interestingly, a higher involvement of the left hemisphere on Aβ load was also found, which is in line with findings from recent studies (Anijärv et al., 2025; Yu et al., 2024). Here we demonstrated in the same sample a matched leftward asymmetrical GM loss and Aβ uptake in functional regions, suggesting that left hemisphere is more susceptible to neuronal injury in early stages of the disease. Despite this hemispheric difference, our results clearly evidence increased 11C-PiB SUVR uptake across all regions of both hemispheres in the AD group compared to the control group, in accordance with previous work (Jack et al., 2008; Klunk et al., 2004).

Between groups comparisons of 11C-PK11195 BP_{ND} data did not show differences in the neuroinflammation levels in any of the visual regions examined. This outcome is consistent with previous work in mild AD that reported enhanced levels of neuroinflammation mainly confined to the temporoparietal and posterior cingulate cortex (Hamelin et al., 2016; Jorge et al., 2021; Kreisl et al., 2013; Yokokura et al., 2011). Moreover, even though microglial activation maybe a key component of the etiopathogenesis of AD, it is believed that its impacts in the brain might fluctuate along with the course of the disease (Fan et al., 2017) and might be either temporally restricted or confined to some brain regions (Bradburn et al., 2019; Edison et al., 2008), which might justify the apparently contradictory findings concerning neuroinflammation in AD (Edison et al., 2008; Groom et al., 1995; Kreisl et al., 2013; Kropholler et al., 2007; Passamonti et al., 2019; Wiley et al., 2009). Normal levels of neuroinflammation may, in fact, have contributed for the overall functional preservation of these areas, as we previously found that increased neuroinflammation, but not Aβ, was negatively associated with functional response in the PCC in AD (Canário et al., 2022).

Studies resorting to fMRI tasks to assess neuronal responses of higher-order visual areas in AD are scarce, though Bokde et al. (2008) could not find group differences in regions involved in face recognition in early AD. Also, Sauer et al. (2006) failed to detect differences in FFA response to a face categorization task between AD patients and controls, converging with the present results. Moreover, a recent study of Canário et al. (2023), where the functional response of seven object recognition areas in AD was investigated, showed a marginal reduction of neuronal activation in right FBA and left VWFA in AD patients.

The lack or minimal significant differences between groups in the aforesaid studies might have resulted from the relatively early stage of the AD samples tested. In fact, several neuropsychological and neuroimaging studies have shown impaired visual cortical activation with AD progression (Adlington et al., 2009; Huang et al., 2021; Kavcic et al., 2011; Mandal et al., 2012; Rizzo et al., 2000). Based on these findings of decreased cortical activation of the visual network as the disease

evolves, it was hypothesized that AD alters this network progressively. This supports the notion that a sequential pathologic effect occurs over time, from higher to lower-order visual association areas, before changes in the early visual cortex (Huang et al., 2021).

Thus, both the sequential temporal order by which the different neuropathological markers evolve, as demonstrated in prior work (Jack et al., 2010; Villemagne et al., 2013), as well as their spatial pattern of accumulation (Huang et al., 2021), might explain the lack of changes in visual function in mild AD. That is, despite these regions being affected in terms of Aβ deposits and neurodegeneration, their functional profile remains unaffected at an early stage. The association found between Aβ and neuronal function specifically in the right LOCv might be explained in light of the previous arguments. Considering that this region is closer to the occipital lobe, it is likely experiencing more recent Aβ accumulation (Albers et al., 2015; Braak and Braak, 1991) compared to the other regions, which is also supported by its bilateral lack of significant atrophy. Speculatively, right LOCv is possibly under Aβ-related neurotoxicity, namely from oligomeric species (Lorenzo and Yankner, 1994; Pike et al., 1995), leading to concurrent synaptic dysfunction (Hardy and Higgins, 1992; Selkoe, 2008), which in turn might induce subtle transient deficits in cognitive function (Cleary et al., 2004), explaining the significant correlation found between activation levels and Aβ in this region. However, given the exploratory nature of the correlation analysis, the present findings should be interpreted with caution.

This temporally dependent subtle transient effect in cognitive function, although insufficient to promote measurable impact on neuronal function as measured by the BOLD response, might somehow trigger the neuropathological downstream cascade occurring later (Hardy and Selkoe, 2002). Accordingly, in Landau et al. (2012)'s study, it was found that Aβ deposition had an early and subclinical impact on cognition (normal aging and early MCI), whereas, at moderate and later stages of disease (later MCI and AD), synaptic and neuronal dysfunction became prominent and more closely linked to the decline in cognitive status. Similar conclusions emerge from studies where relationships between cognition, as assessed by cognitive tests, and 11C-PiB SUVR were limited to the pre-symptomatic stage of AD (Chételat et al., 2012; Pike et al., 2011; Rodrigue et al., 2012) or elderly subjects with augmented Aβ levels (Mormino et al., 2009). Thus, the compelling evidence of a dissociation between Aβ and cognition as AD evolves (Engler et al., 2006; Jack et al., 2009; Landau et al., 2012; Scheinin et al., 2009) might explain the non-existent coupling between Aβ and neuronal activity in other regions, which possibly are in a more advanced phase of the disease, in the neurodegeneration phase per se, contrary to LOCv, which might still be in an early Aβ damage phase. Conversely, numerous studies have found that neurodegeneration is preferentially associated with cognitive dysfunction when AD is established (Savva et al., 2009; Su et al., 2021; Terry et al., 1991; Vemuri et al., 2009a, 2009b). Our results suggest that the brain can handle a certain level of neurodegeneration without consequences to cognitive function (Jack et al., 2011; Jagust, 2018; Sperling et al., 2011). In fact, the brain has an exceptional capacity to accommodate pathological insults without causing functional disturbances (Bateman et al., 2012; Benzinger et al., 2013; Fleisher et al., 2015), and the loss of this functional resilience may be driven by more toxic neuropathological markers, namely neuroinflammation and NFTs.

Overall, our suggestion that Aβ subtly impacts brain function also aligns well with the study by Drzezga et al. (2011), which demonstrated in both 11C-PiB PET positive non-demented healthy subjects and MCI patients that whole-brain connectivity disruptions occurred alongside increased hypometabolism, despite the presence of only very subtle cortical atrophy. They also found negative correlations between Aβ load and both decreased brain connectivity and metabolism, arguing that disruption of functional connectivity between regions may result from synaptic pathologies promoted by Aβ, possibly taking place before neuronal death.

Based on this previous evidence, we hypothesize that by the time Aβ becomes toxic to the brain, it might induce a transient subclinical impact on neuronal function, which in turn may hypothetically trigger the onset of neurodegeneration. These changes precede more visible alterations in cognitive function, which in turn might be reinforced and/or mediated by other neuropathological markers, as neuroinflammation and/or NFTs (Canário et al., 2022; Su et al., 2021). Nevertheless, future longitudinal studies are necessary to test this premise.

As such, the association between neuropathological markers and neuronal function is prone to be dependent on the spatial and temporal spreading of the neuropathological mechanisms throughout the cortical networks, which in turn depends on the stage of the disease, this might indeed explain the controversial evidence linking pathophysiological features in specific brain regions with brain function in AD (Becker et al., 2011; Bourgeat et al., 2010; Cagnin et al., 2001; Dani et al., 2018; Edison et al., 2008; Frisoni et al., 2009; Jorge et al., 2021; McGeer et al., 1987; Okello et al., 2009; Passamonti et al., 2019).

Prior work exploring specifically the associations between pathological traits and visual function in AD had classically resorted to cognitive or psychometric tests. For instance, in the study by Bejanin et al. (2017) it was investigated whether GM density and Aβ pathology contributed to the relationship between tau pathology and cognitive deficits in AD as assessed through specific neuropsychological tests. Their results uphold a decreased cognitive performance in each domain related to increased tau in regions subserving that cognitive function (visuospatial functions: right more than left occipitotemporal regions). Nevertheless, results from this study and ours are hard to compare since we assessed a basic visual function through BOLD activation during the recognition of specific visual stimuli in very specific regions, whereas cognitive tests performed in those studies are known to recruit several regions that are part of more complex networks with functions that go beyond visual recognition. Overall, our findings suggest differential vulnerability to pathological events along the visual ventral stream in AD, corroborating the hypothesis that neuroinflammation is critical across defined temporal windows in the natural history of AD (Canário et al., 2022; Lapo Pais et al., 2023).

Although the sensitivity analysis demonstrates that the results remain broadly stable with the inclusion of Aβ-positive controls, thereby supporting their consistency, some limitations must be considered. For instance, the small sample size reduces statistical power, which not only limits the ability to detect true effects but may also result in inflated effect size estimates due to sampling variability, thereby diminishing the reliability of statistical inferences. Furthermore, although the findings indicate an association between neuropathological changes and brain function in LOCv, the analyses are correlational and do not establish causality or directionality. Future longitudinal research with larger cohorts is necessary to replicate these results and provide more definitive conclusions.

6. Conclusion

In this multimodal study, we were able to infer for the first time about AD-related neuropathological changes in the visual ventral stream and their impact on brain activity, as measured by BOLD fMRI at a mild stage the disease. Remarkably, we found widespread neuropathological changes throughout areas belonging to the ventral stream despite lack of changes in task-related neuronal activity and neuroinflammation. We also found a matched left hemispheric bias for increased Aβ load, extending previous findings on accelerated grey matter loss in this hemisphere. Our data suggests that different networks may have different temporal susceptibility to different neuropathological markers, as shown by the significant negative relationship between Aβ load in right LOCv and brain activity.

CRediT authorship contribution statement

Lília Jorge: Writing – review & editing, Writing – original draft,

Investigation, Conceptualization. **Nádia Canário:** Writing – review & editing, Visualization, Formal analysis. **Ricardo Martins:** Writing – review & editing, Methodology, Formal analysis. **Antero Abrunhosa:** Writing – review & editing, Methodology, Investigation. **Isabel Santana:** Writing – review & editing, Validation, Investigation. **Miguel Castelo-Branco:** Writing – review & editing, Validation, Supervision, Project administration, Funding acquisition, Conceptualization.

Declaration of generative AI and AI-assisted technologies in the writing process

During the preparation of this work, the authors used Microsoft Copilot and Grammarly to assist with English language and grammar improvements. The authors reviewed and edited the content as needed and take full responsibility for the final version of the published article.

Funding sources

This work was supported by grants from the Foundation for Science and Technology, Portugal FCT/UIDB/4950/2025 and FCT/UIDP/4950/2025, 2022.02963.PTDC and individual fellowship to LJ (https://doi.org/10.54499/2020.08187.BD).

Declaration of competing interest

The authors declare that they have no known competing financial interests or personal relationships that could have appeared to influence the work reported in this paper.

Acknowledgements

We acknowledge that some participant data used in this study were previously included in Canário et al. (2023), and we thank the contributors of that work for their foundational efforts.

Glossary:

AD, Alzheimer's disease; Aβ, amyloid-β; fMRI, functional magnetic resonance imaging; FBA, fusiform body area; FFA, fusiform face area; LOCv, lateral occipital cortex; PPA, parahippocampal place area; VWFA, visual word form area; HC, healthy controls; MRI, magnetic resonance imaging; PET, positron emission tomography; PiB, Pittsburgh compound; GM, grey matter; SUVR, standard uptake value ratio; BPND, binding potential; TR, repetition time; TE, echo time; FOV, field of view; MNI, Montreal neurological institute; BOLD, blood oxygen level dependent; FWHM, full width half max; CSF, cerebrospinal fluid; CAT12, Computational Anatomy Toolbox; MPRAGE, Magnetization Prepared Rapid Gradient Echo; ROI, region of interest; SD, standard deviation; TIV, total intracranial volume; WM, white matter; TAL, Talairach reference system; MMSE, Mini Mental State Examination; MoCA, Montreal Cognitive Assessment score, CDR, Clinical Dementia Rating; NFTs, Neurofibrillary tangles.

Appendix A. Supplementary data

Supplementary data to this article can be found online at https://doi.org/10.1016/j.ynirp.2025.100305.

Data availability

Data are available from the corresponding author upon reasonable request.

References

Adlington, R.L., Laws, K.R., Gale, T.M., 2009. Visual processing in Alzheimer's disease: surface detail and colour fail to aid object identification. Neuropsychologia 47 (12), 2574–2583. https://doi.org/10.1016/J.NEUROPSYCHOLOGIA.2009.05.004.

Albers, M.W., Gilmore, G.C., Kaye, J., Murphy, C., Wingfield, A., Bennett, D.A., Boxer, A. L., Buchman, A.S., Cruickshanks, K.J., Devanand, D.P., Duffy, C.J., Gall, C.M., Gates, G.A., Granholm, A.C., Hensch, T., Holtzer, R., Hyman, B.T., Lin, F.R., McKee, A.C., et al., 2015. At the interface of sensory and motor dysfunctions and Alzheimer's disease. Alzheimer's Dementia 11 (1), 70–98. https://doi.org/10.1016/J.JALZ.2014.04.514.

American Psychiatric Association, 2000. Diagnostic and Statistical Manual of Mental Disorders (DSM-IV-TR). Washington, DC.

Anijärv, T.E., Ossenkoppele, R., Smith, R., Pichet Binette, A., Collij, L.E., Behjat, H.H., Rittmo, J., Karlsson, L., Ahmadi, K., Strandberg, O., Weiner, M., Aisen, P., Petersen, R., Jack, C.R., Jagust, W., Landau, S., Rivera-Mindt, M., Okonkwo, O., et al., 2025. Hemispheric asymmetry of tau pathology is related to asymmetric amyloid deposition in Alzheimer's disease. Nat. Commun. 16 (1), 8232. https://doi.org/10.1038/s41467-025-63564-2.

Ashburner, J., 2007. A fast diffeomorphic image registration algorithm. Neuroimage 38 (1), 95–113. https://doi.org/10.1016/J.NEUROIMAGE.2007.07.007.

Ashburner, J., Friston, K.J., 2000. Voxel-based morphometry-the methods. Neuroimage 11, 805–821. https://doi.org/10.1006/nimg.2000.0582.

Ashburner, J., Friston, K.J., 2005. Unified segmentation. Neuroimage 26 (3), 839–851. https://doi.org/10.1016/j.neuroimage.2005.02.018.

Avila, J., Pallas, N., Bolós, M., Sayas, C.L., Hernandez, F., 2016. Intracellular and extracellular microtubule associated protein tau as a therapeutic target in Alzheimer disease and other tauopathies. Expert Opin. Ther. Targets 20 (6), 653–661. https://doi.org/10.1517/14728222.2016.1131269.

Barreto, J., Leuschner, A., Santos, F., Sobral, M., 2008. Escala de Depressão Geriátrica [Geriatric Depressive Scale]. In: Mendonça, C., Garcia, C., Guerreiro, M. (Eds.), Grupo de Estudos de Envelhecimento Cerebral e Demências [Study Group on Brain Aging and Dementia]. Escalas e testes na demência [Scales and tests in dementia], Lisbon, pp. 69–72. GEECD.

Bateman, R.J., Xiong, C., Benzinger, T.L.S., Fagan, A.M., Goate, A., Fox, N.C., Marcus, D. S., Cairns, N.J., Xie, X., Blazey, T.M., Holtzman, D.M., Santacruz, A., Buckles, V., Oliver, A., Moulder, K., Aisen, P.S., Ghetti, B., Klunk, W.E., McDade, E., et al., 2012. Clinical and biomarker changes in dominantly inherited Alzheimer's disease. N. Engl. J. Med. 367 (9), 795–804. https://doi.org/10.1056/NEJMOA1202753.

Baudic, S., Barba, G.D., Thibaudet, M.C., Smagghe, A., Remy, P., Traykov, L., 2006. Executive function deficits in early Alzheimer's disease and their relations with episodic memory. Arch. Clin. Neuropsychol. 21 (1), 15–21. https://doi.org/10.1016/J.ACN.2005.07.002.

Becker, J.A., Hedden, T., Carmasin, J., Maye, J., Rentz, D.M., Putcha, D., Fischl, B., Greve, D.N., Marshall, G.A., Salloway, S., Marks, D., Buckner, R.L., Sperling, R.A., Johnson, K.A., 2011. Amyloid-β associated cortical thinning in clinically normal elderly. Ann. Neurol. 69 (6), 1032–1042. https://doi.org/10.1002/ana.22333.

Bejanin, A., Schonhaut, D.R., La Joie, R., Kramer, J.H., Baker, S.L., Sosa, N., Ayakta, N., Cantwell, A., Janabi, M., Lauriola, M., O'Neil, J.P., Gorno-Tempini, M.L., Miller, Z. A., Rosen, H.J., Miller, B.L., Jagust, W.J., Rabinovici, G.D., 2017. Tau pathology and neurodegeneration contribute to cognitive impairment in Alzheimer's disease. Brain 140 (12), 3286–3300. https://doi.org/10.1093/BRAIN/AWX243.

Benzinger, T.L.S., Blazey, T., Jack, C.R., Koeppe, R.A., Su, Y., Xiong, C., Raichle, M.E., Snyder, A.Z., Ances, B.M., Bateman, R.J., Cairns, N.J., Fagan, A.M., Goate, A., Marcus, D.S., Aisen, P.S., Christensen, J.J., Ercole, L., Hornbeck, R.C., Farrar, A.M., et al., 2013. Regional variability of imaging biomarkers in autosomal dominant Alzheimer's disease. Proc. Natl. Acad. Sci. U. S. A 110 (47). https://doi.org/10.1073/PNAS.1317918110.

Bloom, G.S., 2014. Amyloid-β and tau the trigger and bullet in alzheimer disease pathogenesis. JAMA Neurol. 71 (4), 505–508.

Bokde, A.L.W., Lopez-Bayo, P., Born, C., Dong, W., Meindl, T., Leinsinger, G., Teipel, S.J., Faltraco, F., Reiser, M., Möller, H.J., Hampel, H., 2008. Functional abnormalities of the visual processing system in subjects with mild cognitive impairment: an fMRI study. Psychiatr. Res. Neuroimaging 163 (3), 248–259. https://doi.org/10.1016/J.PSCYCHRESNS.2007.08.013.

Bonilla, J.F., Carril, J.M., 2013. Molecular neuroimaging in degenerative dementias. Rev. Española Med. Nucl. Imagen Mol. 32 (5), 301–309. https://doi.org/10.1016/J.REMNIE.2013.07.027.

Bourgeat, P., Chetelat, G., Villemagne, V.L., Fripp, J., Raniga, P., Pike, K., Acosta, O., Szoeke, C., Ourselin, S., Ames, D., Ellis, K.A., Martins, R.N., Masters, C.L., Rowe, C. C., Salvado, O., AIBL Research Group, 2010. Beta-amyloid burden in the temporal neocortex is related to hippocampal atrophy in elderly subjects without dementia. Neurology 74 (2), 121–127. https://doi.org/10.1212/WNL.0b013e3181c918b5.

Braak, H., Braak, E., 1991. Neuropathological stageing of alzheimer-related changes. Acta Neuropathol. 82 (4), 239–259. https://doi.org/10.1007/BF00308809.

Bradburn, S., Murgatroyd, C., Ray, N., 2019. Neuroinflammation in mild cognitive impairment and Alzheimer's disease: a meta-analysis. Ageing Res. Rev. 50, 1–8. https://doi.org/10.1016/J.ARR.2019.01.002.

Busatto, G.F., Diniz, B.S., Zanetti, M.V., 2008. Voxel-based morphometry in Alzheimer's disease. Expert Rev. Neurother. 8 (11), 1691–1702. https://doi.org/10.1586/14737175.8.11.1691.

Busatto, G.F., Garrido, G.E.J., Almeida, O.P., Castro, C.C., Camargo, C.H.P., Cid, C.G., Buchpiguel, C.A., Furuie, S., Bottino, C.M., 2003. A voxel-based morphometry study of temporal lobe gray matter reductions in Alzheimer's disease. Neurobiol. Aging 24 (2), 221–231. https://doi.org/10.1016/S0197-4580(02)00084-2.

Cagnin, A., Brooks, D.J., Kennedy, A.M., Gunn, R.N., Myers, R., Turkheimer, F.E., Jones, T., Banati, R.B., 2001. In-vivo measurement of activated microglia in dementia. Lancet 358 (9280), 461–467. https://doi.org/10.1016/S0140-6736(01)05625-2.

Canário, N., Jorge, L., Martins, R., Santana, I., Castelo-Branco, M., 2022. Dual PET-fMRI reveals a link between neuroinflammation, amyloid binding and compensatory task-related brain activity in Alzheimer's disease. Commun. Biol. 5 (1), 804. https://doi.org/10.1038/s42003-022-03761-7.

Canário, N., Jorge, L., Silva, M.F.L., Alberto, M., Castelo-branco, M., 2016. Neuropsychologia Distinct preference for spatial frequency content in ventral stream regions underlying the recognition of scenes , faces , bodies and other objects. Neuropsychologia 87, 110–119. https://doi.org/10.1016/j.neuropsychologia.2016.05.010.

Canário, N.S., Jorge, L.P., Santana, I.J., Castelo-Branco, M.S., 2023. Hemispheric patterns of recruitment of object processing regions in early alzheimer's disease: a study along the entire ventral stream. J. Alzheim. Dis. 91 (3), 1151–1164. https://doi.org/10.3233/JAD-220055.

Chételat, G., Desgranges, B., de la Sayette, V., Viader, F., Eustache, F., Baron, J.-C., 2002. Mapping gray matter loss with voxel-based morphometry in mild cognitive impairment. Neuroreport 13 (15), 1939–1943. https://doi.org/10.1097/00001756-200210280-00022.

Chételat, G., Villemagne, V.L., Pike, K.E., Ellis, K.A., Ames, D., Masters, C.L., Rowe, C.C., 2012. Relationship between memory performance and β-Amyloid deposition at different stages of alzheimer's disease. Neurodegener. Dis. 10 (1–4), 141–144. https://doi.org/10.1159/000334295.

Cichy, R.M., Chen, Y., Haynes, J.D., 2011. Encoding the identity and location of objects in human LOC. Neuroimage 54 (3), 2297–2307. https://doi.org/10.1016/J.NEUROIMAGE.2010.09.044.

Cleary, J.P., Walsh, D.M., Hofmeister, J.J., Shankar, G.M., Kuskowski, M.A., Selkoe, D.J., Ashe, K.H., 2004. Natural oligomers of the amyloid-β protein specifically disrupt cognitive function. Nat. Neurosci. 8 (1), 79–84. https://doi.org/10.1038/nn1372.

Dani, M., Wood, M., Mizoguchi, R., Fan, Z., Walker, Z., Morgan, R., Hinz, R., Biju, M., Kuruvilla, T., Brooks, D.J., Edison, P., 2018. Microglial activation correlates in vivo with both tau and amyloid in Alzheimer's disease. Brain 141 (9), 2740–2754. https://doi.org/10.1093/brain/awy188.

Davies-Thompson, J., Johnston, S., Tashakkor, Y., Pancaroglu, R., Barton, J.J.S., 2016. The relationship between visual word and face processing lateralization in the fusiform gyri: a cross-sectional study. Brain Res. 1644, 88–97. https://doi.org/10.1016/j.brainres.2016.05.009.

Done, D.J., Hajilou, B.B., 2005. Loss of high-level perceptual knowledge of object structure in DAT. Neuropsychologia 43 (1), 60–68. https://doi.org/10.1016/j.neuropsychologia.2004.06.004.

Downing, P.E., Peelen, M.V., 2011. The role of occipitotemporal body-selective regions in person perception. Cognit. Neurosci. 2 (3–4), 186–203. https://doi.org/10.1080/17588928.2011.582945.

Drzezga, A., Becker, J.A., Van Dijk, K.R.A., Sreenivasan, A., Talukdar, T., Sullivan, C., Schultz, A.P., Sepulcre, J., Putcha, D., Greve, D., Johnson, K.A., Sperling, R.A., 2011. Neuronal dysfunction and disconnection of cortical hubs in non-demented subjects with elevated amyloid burden. Brain 134 (6), 1635–1646. https://doi.org/10.1093/BRAIN/AWR066.

Edison, P., Archer, H.A., Gerhard, A., Hinz, R., Pavese, N., Turkheimer, F.E., Hammers, A., Tai, Y.F., Fox, N., Kennedy, A., Rossor, M., Brooks, D.J., 2008. Microglia, amyloid, and cognition in Alzheimer's disease: an [11C](R)PK11195-PET and [11C]PIB-PET study. Neurobiol. Dis. 32 (3), 412–419. https://doi.org/10.1016/J.NBD.2008.08.001.

Engler, H., Forsberg, A., Almkvist, O., Blomquist, G., Larsson, E., Savitcheva, I., Wall, A., Ringheim, A., Langstrom, B., Nordberg, A., 2006. Two-year follow-up of amyloid deposition in patients with Alzheimer's disease. Brain 129 (11), 2856–2866. https://doi.org/10.1093/brain/awl178.

Fan, Z., Brooks, D.J., Okello, A., Edison, P., 2017. An early and late peak in microglial activation in Alzheimer's disease trajectory. Brain 140 (3), 792–803. https://doi.org/10.1093/brain/aww349.

Ferman, T.J., Smith, G.E., Boeve, B.F., Graff-Radford, N.R., Lucas, J.A., Knopman, D.S., Petersen, R.C., Ivnik, R.J., Wszolek, Z., Uitti, R., Dickson, D.W., 2006. Neuropsychological differentiation of dementia with lewy bodies from normal aging and Alzheimer's disease. Clin. Neuropsychol. 20 (4), 623–636. https://doi.org/10.1080/13854040500376831.

Fleisher, A.S., Chen, K., Quiroz, Y.T., Jakimovich, L.J., Gutierrez Gomez, M., Langois, C. M., Langbaum, J.B.S., Roontiva, A., Thiyyagura, P., Lee, W., Ayutyanont, N., Lopez, L., Moreno, S., Muñoz, C., Tirado, V., Acosta-Baena, N., Fagan, A.M., Giraldo, M., Garcia, G., et al., 2015. Associations between biomarkers and age in the presenilin 1 E280A autosomal dominant Alzheimer disease kindred: a cross-sectional study. JAMA Neurol. 72 (3), 316–324. https://doi.org/10.1001/JAMANEUROL.2014.3314.

Freitas, S., Simões, M.R., Alves, L., Santana, I., 2011. Montreal cognitive assessment (MoCA): normative study for the Portuguese population. J. Clin. Exp. Neuropsychol. 33 (9), 989–996. https://doi.org/10.1080/13803395.2011.589374.

Frisoni, G.B., Lorenzi, M., Caroli, A., Kemppainen, N., Någren, K., Rinne, J.O., 2009. In vivo mapping of amyloid toxicity in Alzheimer disease. Neurology 72 (17), 1504–1511. https://doi.org/10.1212/WNL.0b013e3181a2e896.

Ginó, S., Mendes, T., Ribeiro, F., Mendonça, A., Guerreiro, M., Garcia, C., 2008. Escala de Queixas de Memória [Subjective Memory Complaints]. In: Mendonça, C., Garcia, C., Guerreiro, M. (Eds.), Grupo de Estudos de Envelhecimento Cerebral e Demências [Study Group on Brain Aging and Dementia]. Escalas e testes na demência [Scales and tests in dementia], Lisbon, pp. 116–120. GEECD.

Goebel, R., Esposito, F., Formisano, E., 2006. Analysis of functional image analysis contest (FIAC) data with brainvoyager QX: From single-subject to cortically aligned group general linear model analysis and self-organizing group independent component analysis. Human Brain Mapping 27 (5), 392–401. https://doi.org/10.1002/hbm.20249.

Graewe, B., Lemos, R., Ferreira, C., Santana, I., Farivar, R., De Weerd, P., Castelo-Branco, M., 2013. Impaired processing of 3D motion-defined faces in mild cognitive impairment and healthy aging: an fMRI study. Cerebr. Cortex 23 (10), 2489–2499. https://doi.org/10.1093/CERCOR/BHS246.

Grill-Spector, K., Knouf, N., Kanwisher, N., 2004. The fusiform face area subserves face perception, not generic within-category identification. Nat. Neurosci. 7 (5), 555–562. https://doi.org/10.1038/nn1224.

Grill-Spector, K., Kourtzi, Z., Kanwisher, N., 2001. The lateral occipital complex and its role in object recognition. Vis. Res. 41 (10–11), 1409–1422. https://doi.org/10.1016/S0042-6989(01)00073-6.

Groom, G., Junck, L., Foster, N.L., Frey, K.A., Kuhl, D.E., 1995. PET of peripheral benzodiazepine binding sites in the microgliosis of Alzheimer's disease. J. Nucl. Med. 36, 2207–2210.

Hamelin, L., Lagarde, J., Dorothée, G., Leroy, C., Labit, M., Comley, R.A., de Souza, L.C., Corne, H., Dauphinot, L., Bertoux, M., Dubois, B., Gervais, P., Colliot, O., Potier, M. C., Bottlaender, M., Sarazin, M., 2016. Early and protective microglial activation in Alzheimer's disease: a prospective study using 18F-DPA-714 PET imaging. Brain 139 (4), 1252–1264. https://doi.org/10.1093/brain/aww017.

Hardy, J., Higgins, G., 1992. Alzheimer's disease: the amyloid cascade hypothesis. Science 256 (5054), 184–185. https://doi.org/10.1126/science.1566067.

Hardy, J., Selkoe, D., 2002. The amyloid hypothesis of Alzheimer's disease: progress and problems on the road to therapeutics. Science 297 (5580), 353–356.

Haxby, J.V., Grady, C.L., Horwitz, B., Ungerleider, L.G., Mishkin, M., Carson, R.E., Herscovitch, P., Schapiro, M.B., Rapoport, S.I., 1991. Dissociation of object and spatial visual processing pathways in human extrastriate cortex. Proceed. National Academy Scie. U.S.A 88 (5), 1621–1625. https://doi.org/10.1073/PNAS.88.5.1621.

Hrybouski, S., Das, S.R., Xie, L., Lyu, X., Wisse, L.E.M., Kelley, M., Lane, J., Sherin, M., DiCalogero, M., Nasrallah, I.M., Detre, J.A., Yushkevich, P.A., Wolk, D.A., 2024. BOLD fMRI signal changes in preclinical Alzheimer's disease. Alzheimer's Dementia 20 (S9), e094155. https://doi.org/10.1002/alz.094155.

Huang, J., Beach, P., Bozoki, A., Zhu, D.C., 2021. Alzheimer's disease progressively reduces visual functional network connectivity. J. Alzheimer's Disease Rep. 5 (1), 549–562. https://doi.org/10.3233/ADR-210017.

Ichise, M., Liow, J.-S., Lu, J.-Q., Takano, A., Model, K., Toyama, H., Suhara, T., Suzuki, K., Innis, R.B., Carson, R.E., 2003. Linearized reference tissue parametric imaging methods: application to [11C]DASB positron emission tomography studies of the serotonin transporter in human brain. J. Cerebr. Blood Flow Metabol. 23 (9), 1096–1112. https://doi.org/10.1097/01.WCB.0000085441.37552. CA.

Jack, C.R., Albert, M.S., Knopman, D.S., McKhann, G.M., Sperling, R.A., Carrillo, M.C., Thies, B., Phelps, C.H., 2011. Introduction to the recommendations from the national institute on aging-alzheimer's association workgroups on diagnostic guidelines for Alzheimer's disease. Alzheimer's Dementia : J. Alzheimer's Associat. 7 (3), 257–262. https://doi.org/10.1016/J.JALZ.2011.03.004.

Jack, C.R., Knopman, D.S., Jagust, W.J., Shaw, L.M., Aisen, P.S., Weiner, M.W., Petersen, R.C., Trojanowski, J.Q., 2010. Hypothetical model of dynamic biomarkers of the Alzheimer's pathological Cascade. Lancet Neurol. 9 (1), 119–128. https://doi.org/10.1016/S1474-4422(09)70299-6.

Jack, C.R., Lowe, V.J., Senjem, M.L., Weigand, S.D., Kemp, B.J., Shiung, M.M., Knopman, D.S., Boeve, B.F., Klunk, W.E., Mathis, C.A., Petersen, R.C., 2008. 11C PiB and structural MRI provide complementary information in imaging of Alzheimer's disease and amnestic mild cognitive impairment. Brain 131 (3), 665–680. https://doi.org/10.1093/brain/awm336.

Jack, C.R., Lowe, V.J., Weigand, S.D., Wiste, H.J., Senjem, M.L., Knopman, D.S., Shiung, M.M., Gunter, J.L., Boeve, B.F., Kemp, B.J., Weiner, M., Petersen, R.C., 2009. Serial PIB and MRI in normal, mild cognitive impairment and Alzheimer's disease: implications for sequence of pathological events in Alzheimer's disease. Brain 132 (5), 1355–1365. https://doi.org/10.1093/brain/awp062.

Jagust, W., 2018. Imaging the evolution and pathophysiology of Alzheimer disease. Nat. Rev. Neurosci. 19 (11), 687. https://doi.org/10.1038/S41583-018-0067-3.

Jorge, L., Canário, N., Castelhano, J., Castelo-Branco, M., 2018. Processing of performance-matched visual object categories: faces and places are related to lower processing load in the frontoparietal executive network than other objects. Eur. J. Neurosci. 47 (February), 938–946. https://doi.org/10.1111/ejn.13892.

Jorge, L., Martins, R., Canário, N., Xavier, C., Abrunhosa, A., Santana, I., Castelo-Branco, M., 2021. Investigating the spatial associations between Amyloid-β deposition, grey matter volume, and neuroinflammation in Alzheimer's disease. J. Alzheim. Dis. : JAD 80 (1), 113–132. https://doi.org/10.3233/JAD-200840.

Kavcic, V., Vaughn, W., Duffy, C.J., 2011. Distinct visual motion processing impairments in aging and Alzheimer's disease. Vis. Res. 51 (3), 386–395. https://doi.org/10.1016/J.VISRES.2010.12.004.

Kikinis, R., Pieper, S.D., Vosburgh, K.G., 2014. 3D slicer: a platform for subject-specific image analysis, visualization, and clinical support. In: Jolesz, F.A. (Ed.), Intraoperative Imaging and Image-Guided Therapy. Springer, New York, pp. 277–289. https://doi.org/10.1007/978-1-4614-7657-3_19.

Klunk, W.E., Engler, H., Nordberg, A., Wang, Y., Blomqvist, G., Holt, D.P., Bergström, M., Savitcheva, I., Huang, G.-F., Estrada, S., Ausén, B., Debnath, M.L., Barletta, J., Price, J.C., Sandell, J., Lopresti, B.J., Wall, A., Koivisto, P., Antoni, G., et al., 2004. Imaging brain amyloid in Alzheimer's disease with Pittsburgh Compound-B. Ann. Neurol. 55 (3), 306–319. https://doi.org/10.1002/ana.20009.

Kreisl, W.C., Lyoo, C.H., McGwier, M., Snow, J., Jenko, K.J., Kimura, N., Corona, W., Morse, C.L., Zoghbi, S.S., Pike, V.W., McMahon, F.J., Turner, R.S., Innis, R.B., 2013.

In vivo radioligand binding to translocator protein correlates with severity of Alzheimer's disease. Brain 136 (7), 2228–2238. https://doi.org/10.1093/brain/awt145.

Kropholler, M.A., Boellaard, R., van Berckel, B.N., Schuitemaker, A., Kloet, R.W., Lubberink, M.J., Jonker, C., Scheltens, P., Lammertsma, A.A., 2007. Evaluation of reference regions for (R) -[11C]PK11195 studies in Alzheimer's disease and mild cognitive impairment. J. Cerebr. Blood Flow Metabol. 27 (12), 1965–1974. https://doi.org/10.1038/sj.jcbfm.9600488.

Kuczynski, B., Targan, E., Madison, C., Weiner, M., Zhang, Y., Reed, B., Chui, H.C., Jagust, W., 2010. White matter integrity and cortical metabolic associations in aging and dementia. Alzheimer's Dementia 6 (1), 54–62. https://doi.org/10.1016/J.JALZ.2009.04.1228.

Landau, S.M., Mintun, M.A., Joshi, A.D., Koeppe, R.A., Petersen, R.C., Aisen, P.S., Weiner, M.W., Jagust, W.J., 2012. Amyloid deposition, hypometabolism, and longitudinal cognitive decline. Ann. Neurol. 72 (4), 578–586. https://doi.org/10.1002/ANA.23650/ABSTRACT.

Lapo Pais, M., Jorge, L., Martins, R., Canário, N., Xavier, A.C., Bernardes, R., Abrunhosa, A., Santana, I., Castelo-Branco, M., 2023. Textural properties of microglial activation in Alzheimer's disease as measured by (R)-[11C]PK11195 PET. Brain Commun. 5 (3), fcad148. https://doi.org/10.1093/braincomms/fcad148.

Lawton, M.P., Brody, E.M., 1969. Assessment of older people: self-maintaining and instrumental activities of daily living. Gerontologist 9, 179–186.

Liu, C., Zhang, W.T., Tang, Y.Y., Mai, X.Q., Chen, H.C., Tardif, T., Luo, Y.J., 2008. The visual word form area: evidence from an fMRI study of implicit processing of Chinese characters. Neuroimage 40 (3), 1350–1361. https://doi.org/10.1016/J.NEUROIMAGE.2007.10.014.

Lo, C.Y., Wang, P.N., Chou, K.H., Wang, J., He, Y., Lin, C.P., 2010. Diffusion tensor tractography reveals abnormal topological organization in structural cortical networks in Alzheimer's disease. J. Neurosci. 30 (50), 16876–16885. https://doi.org/10.1523/JNEUROSCI.4136-10.2010.

Lorenzo, A., Yankner, B.A., 1994. Beta-amyloid neurotoxicity requires fibril formation and is inhibited by Congo red. Proc. Natl. Acad. Sci. 91 (25), 12243–12247. https://doi.org/10.1073/PNAS.91.25.12243.

Madureira, S., Verdelho, A., 2008. Escala de Actividades Instrumentais de Vida Diária [Instrumental Activities of Daily Living]. In: Mendonça, C., Garcia, C., Guerreiro, M. (Eds.), Grupo de Estudos de Envelhecimento Cerebral e Demências [Study Group on Brain Aging and Dementia]. Escalas e testes na demência [Scales and tests in dementia], Lisbon, pp. 121–124. GEECD.

Mandal, P.K., Joshi, J., Saharan, S., 2012. Visuospatial perception: an emerging biomarker for Alzheimer's disease. J. Alzheim. Dis. 31 (s3), S117–S135. https://doi.org/10.3233/JAD-2012-120901.

Marshall, G.A., Rentz, D.M., Frey, M.T., Locascio, J.J., Johnson, K.A., Sperling, R.A., 2011. Executive function and instrumental activities of daily living in mild cognitive impairment and Alzheimer's disease. Alzheimer's Dementia 7 (3), 300–308. https://doi.org/10.1016/J.JALZ.2010.04.005.

Matsuda, H., 2013. Voxel-based morphometry of brain MRI in normal aging and Alzheimer's disease. Aging Disease 4 (1), 29–37.

McDonald, C.R., McEvoy, L.K., Gharapetian, L., Fennema-Notestine, C., Hagler, D.J., Holland, D., Koyama, A., Brewer, J.B., Dale, A.M., Alzheimer's Disease Neuroimaging Initiative, 2009. Regional rates of neocortical atrophy from normal aging to early Alzheimer disease. Neurology 73 (6), 457–465. https://doi.org/10.1212/WNL.0b013e3181b16431.

McGeer, P.L., Itagaki, S., Tago, H., McGeer, E.G., 1987. Reactive microglia in patients with senile dementia of the Alzheimer type are positive for the histocompatibility glycoprotein HLA-DR. Neurosci. Lett. 79 (1–2), 195–200. https://doi.org/10.1016/0304-3940(87)90696-3.

McKhann, G.M., Knopman, D.S., Chertkow, H., Hyman, B.T., Jack, C.R., Kawas, C.H., Klunk, W.E., Koroshetz, W.J., Manly, J.J., Mayeux, R., Mohs, R.C., Morris, J.C., Rossor, M.N., Scheltens, P., Carrillo, M.C., Thies, B., Weintraub, S., Phelps, C.H., 2011. The diagnosis of dementia due to Alzheimer's disease: recommendations from the national institute on Aging-Alzheimer's association workgroups on diagnostic guidelines for Alzheimer's disease. Alzheimer's Dementia 7 (3), 263–269. https://doi.org/10.1016/J.JALZ.2011.03.005.

McNamee, R.L., Yee, S.-H., Price, J.C., Klunk, W.E., Rosario, B., Weissfeld, L., Ziolko, S., Berginc, M., Lopresti, B., Dekosky, S., Mathis, C.A., 2009. Consideration of optimal time window for Pittsburgh compound B PET summed uptake measurements. J. Nucl. Med. : Off. Publ. Soc. Nuclear Med. 50 (3), 348–355. https://doi.org/10.2967/jnumed.108.057612.

Mendez, M.F., Ghajarania, M., Perryman, K.M., 2002. Posterior cortical atrophy: clinical characteristics and differences compared to Alzheimer's disease. Dement. Geriatr. Cognit. Disord. 14 (1), 33–40. https://doi.org/10.1159/000058331.

Minkova, L., Habich, A., Peter, J., Kaller, C.P., Eickhoff, S.B., Klöppel, S., 2017. Gray matter asymmetries in aging and neurodegeneration: a review and meta-analysis. Hum. Brain Mapp. 38 (12), 5890–5904. https://doi.org/10.1002/hbm.23772.

Mishkin, M., Ungerleider, L.G., Macko, K.A., 1983. Object vision and spatial vision: two cortical pathways. Trends Neurosci. 6 (C), 414–417. https://doi.org/10.1016/0166-2236(83)90190-X.

Mormino, E.C., Kluth, J.T., Madison, C.M., Rabinovici, G.D., Baker, S.L., Miller, B.L., Koeppe, R.A., Mathis, C.A., Weiner, M.W., Jagust, W.J., 2009. Episodic memory loss is related to hippocampal-mediated B -amyloid deposition in elderly subjects. Brain 132 (5), 1310–1323. https://doi.org/10.1093/brain/awn320.

Okello, A., Edison, M.P., Archer, M.H., Turkheimer, M.F., Kennedy, J., Bullock, M.R., Walker, Mrcp Z., Kennedy, A., Fox, N., Rossor, M., Brooks, Ds D., 2009. Microglial activation and amyloid deposition in mild cognitive impairment A PET study. Neurology 72 (6), 56–62.

Oliveira, F., Leuzy, A., Castelhano, J., Chiotis, K., Hasselbalch, S.G., Rinne, J., Mendonça, A., Otto, M., Lleó, A., Santana, I., Johansson, J., Anderl-Straub, S., Arnim, C., Beer, A., Blesa, R., Fortea, J., Sanna-Kaisa, H., Portelius, E., Pannee, J., et al., 2018. Data driven diagnostic classification in Alzheimer's disease based on different reference regions for normalization of PiB-PET images and correlation with CSF concentrations of Aβ species. Neuroimage: Clinical 20, 603–610. https://doi.org/10.1016/J.NICL.2018.08.023.

Pasqualetti, G., Brooks, D.J., Edison, P., 2015. The role of neuroinflammation in dementias. Curr. Neurol. Neurosci. Rep. 15 (4), 17. https://doi.org/10.1007/s11910-015-0531-7.

Passamonti, L., Tsvetanov, K.A., Jones, P.S., Bevan-Jones, W.R., Arnold, R., Borchert, R. J., Mak, E., Su, L., O'Brien, J.T., Rowe, J.B., 2019. Neuroinflammation and functional connectivity in Alzheimer's disease: interactive influences on cognitive performance. J. Neurosci. 39 (36), 7218–7226. https://doi.org/10.1523/JNEUROSCI.2574-18.2019.

Pihlajamäki, M., Tanila, H., Könönen, M., Hänninen, T., Aronen, H.J., Soininen, H., 2005. Distinct and overlapping fMRI activation networks for processing of novel identities and locations of objects. Eur. J. Neurosci. 22 (8), 2095–2105. https://doi.org/10.1111/J.1460-9568.2005.04380.X.

Pike, C.J., Walencewicz-Wasserman, A.J., Kosmoski, J., Cribbs, D.H., Glabe, C.G., Cotman, C.W., 1995. Structure-activity analyses of β-Amyloid peptides: contributions of the β25–35 region to aggregation and neurotoxicity. J. Neurochem. 64 (1), 253–265. https://doi.org/10.1046/J.1471-4159.1995.64010253.X.

Pike, K.E., Ellis, K.A., Villemagne, V.L., Good, N., Chételat, G., Ames, D., Szoeke, C., Laws, S.M., Verdile, G., Martins, R.N., Masters, C.L., Rowe, C.C., 2011. Cognition and beta-amyloid in preclinical Alzheimer's disease: data from the AIBL study. Neuropsychologia 49 (9), 2384–2390. https://doi.org/10.1016/J.NEUROPSYCHOLOGIA.2011.04.012.

Raj, A., Kuceyeski, A., Weiner, M., 2012. A network diffusion model of disease progression in dementia. Neuron 73 (6), 1204–1215. https://doi.org/10.1016/J.NEURON.2011.12.040.

Rizzo, M., Anderson, S.W., Dawson, J., Nawrot, M., 2000. Vision and cognition in Alzheimer's disease. Neuropsychologia 38 (8), 1157–1169. https://doi.org/10.1016/S0028-3932(00)00023-3.

Rodrigue, K.M., Kennedy, K.M., Devous, M.D., Rieck, J.R., Hebrank, A.C., Diaz-Arrastia, R., Mathews, D., Park, D.C., 2012. β-Amyloid burden in healthy aging. Neurology 78 (6), 387–395. https://doi.org/10.1212/WNL.0B013E318245D295.

Roe, J.M., Vidal-Piñeiro, D., Sørensen, Ø., Brandmaier, A.M., Düzel, S., Gonzalez, H.A., Kievit, R.A., Knights, E., Kühn, S., Lindenberger, U., Mowinckel, A.M., Nyberg, L., Park, D.C., Pudas, S., Rundle, M.M., Walhovd, K.B., Fjell, A.M., Westerhausen, R., , The Australian Imaging Biomarkers and Lifestyle Flagship Study of Ageing, Vacher, M., et al., 2021. Asymmetric thinning of the cerebral cortex across the adult lifespan is accelerated in Alzheimer's disease. Nat. Commun. 12 (1), 721. https://doi.org/10.1038/s41467-021-21057-y.

Sauer, J., Ffytche, D.H., Ballard, C., Brown, R.G., Howard, R., 2006. Differences between Alzheimer's disease and dementia with lewy bodies: an fMRI study of task-related brain activity. Brain 129 (7), 1780–1788. https://doi.org/10.1093/BRAIN/AWL102.

Savva, G.M., Wharton, S.B., Ince, P.G., Forster, G., Matthews, F.E., Brayne, C., 2009. Age, neuropathology, and dementia. N. Engl. J. Med. 360 (22), 2302–2309. https://doi.org/10.1056/NEJMOA0806142/SUPPL_FILE/NEJM_SAVVA_2302SA1.PDF.

Scheinin, N.M., Aalto, S., Koikkalainen, J., Lotjonen, J., Karrasch, M., Kemppainen, N., Viitanen, M., Nagren, K., Helin, S., Scheinin, M., Rinne, J.O., 2009. Follow-up of [11C]PIB uptake and brain volume in patients with alzheimer disease and controls. Neurology 73 (15), 1186–1192. https://doi.org/10.1212/WNL.0b013e3181bacf1b.

Schmand, B., Jonker, C., Hooijer, C., Lindeboom, J., 1996. Subjective memory complaints may announce dementia. Neurology 46 (1), 121–125.

Selkoe, D., 2004. Cell biology of protein misfolding: the examples of Alzheimer's and Parkinson's diseases. Nat. Cell Biol. 6 (11), 1054–1061.

Selkoe, D.J., 2008. Soluble oligomers of the amyloid β-Protein: impair synaptic plasticity and behavior. In: Synaptic Plasticity and the Mechanism of Alzheimer's Disease. Springer, Berlin, Heidelberg, pp. 89–102. https://doi.org/10.1007/978-3-540-76330-7_8.

Sereno, M.I., Dale, A.M., Reppas, J.B., Kwong, K.K., Belliveau, J.W., Brady, T.J., Rosen, B.R., Tootell, R.B.H., 1995. Borders of multiple visual areas in humans revealed by functional magnetic resonance imaging. Science 268 (5212), 889–893. https://doi.org/10.1126/SCIENCE.7754376.

Sperling, R.A., Aisen, P.S., Beckett, L.A., Bennett, D.A., Craft, S., Fagan, A.M., Iwatsubo, T., Jack, C.R., Kaye, J., Montine, T.J., Park, D.C., Reiman, E.M., Rowe, C. C., Siemers, E., Stern, Y., Yaffe, K., Carrillo, M.C., Thies, B., Morrison-Bogorad, M., et al., 2011. Toward defining the preclinical stages of Alzheimer's disease: recommendations from the national institute on Aging-Alzheimer's association workgroups on diagnostic guidelines for Alzheimer's disease. Alzheimer's Dementia : J. Alzheimer's Associat. 7 (3), 280. https://doi.org/10.1016/J.JALZ.2011.03.003.

Su, L., Surendranathan, A., Huang, Y., Bevan-Jones, W.R., Passamonti, L., Hong, Y.T., Arnold, R., Rodríguez, P.V., Wang, Y., Mak, E., Fryer, T.D., Aigbirhio, F., Rowe, J.B., O'Brien, J.T., 2021. Relationship between tau, neuroinflammation and atrophy in Alzheimer's disease: the NIMROD study. Inf. Fusion 67 (October 2020), 116–124. https://doi.org/10.1016/j.inffus.2020.10.006.

Terry, R.D., Masliah, E., Salmon, D.P., Butters, N., DeTeresa, R., Hill, R., Hansen, L.A., Katzman, R., 1991. Physical basis of cognitive alterations in alzheimer's disease: synapse loss is the major correlate of cognitive impairment. Ann. Neurol. 30 (4), 572–580. https://doi.org/10.1002/ANA.410300410.

Thompson, E., Schroder, A., He, T., Shand, C., Soskic, S., Oxtoby, N.P., Barkhof, F., Alexander, D.C., for the Alzheimer's Disease Neuroimaging Initiative, 2024. Combining multimodal connectivity information improves modelling of pathology

spread in Alzheimer's disease. Imag . Neurosci. 2. https://doi.org/10.1162/imag_a_00089 imag–2–00089.
Tyler, C., Likova, L., Chen, C.-C., Kontsevich, L., Schira, M., Wade, A., 2005. Extended concepts of occipital retinotopy. Curr. Med. Imag. Rev. 1 (3), 319–329. https://doi.org/10.2174/157340505774574772.
Vemuri, P., Wiste, H.J., Weigand, S.D., Shaw, L.M., Trojanowski, J.Q., Weiner, M.W., Knopman, D.S., Petersen, R.C., Jack, C.R., 2009a. MRI and CSF biomarkers in normal, MCI, and AD subjects: diagnostic discrimination and cognitive correlations. Neurology 73 (4), 287–293. https://doi.org/10.1212/WNL.0B013E3181AF79E5.
Vemuri, P., Wiste, H.J., Weigand, S.D., Shaw, L.M., Trojanowski, J.Q., Weiner, M.W., Knopman, D.S., Petersen, R.C., Jack, C.R., 2009b. MRI and CSF biomarkers in normal, MCI, and AD subjects: predicting future clinical change. Neurology 73 (4), 294–301. https://doi.org/10.1212/WNL.0B013E3181AF79FB.
Villemagne, V.L., Burnham, S., Bourgeat, P., Brown, B., Ellis, K.A., Salvado, O., Szoeke, C., Macaulay, S.L., Martins, R., Maruff, P., Ames, D., Rowe, C.C., Masters, C. L., 2013. Amyloid β deposition, neurodegeneration, and cognitive decline in sporadic Alzheimer's disease: a prospective cohort study. Lancet Neurol. 12 (4), 357–367. https://doi.org/10.1016/S1474-4422(13)70044-9.
Wandell, B.A., Brewer, A.A., Dougherty, R.F., 2005. Visual field map clusters in human cortex. Phil. Trans. Biol. Sci. 360 (1456), 693–707. https://doi.org/10.1098/RSTB.2005.1628.
Whitwell, J.L., 2010. Progression of atrophy in Alzheimer's disease and related disorders. Neurotox. Res. 18 (3–4), 339–346. https://doi.org/10.1007/s12640-010-9175-1.
Wiley, C.A., Lopresti, B.J., Venneti, S., Price, J., Klunk, W.E., DeKosky, S.T., Mathis, C.A., 2009. Carbon 11–Labeled Pittsburgh compound B and carbon 11–Labeled (R)-PK11195 positron emission tomographic imaging in alzheimer disease. Arch. Neurol. 66 (1), 60–67. https://doi.org/10.1001/archneurol.2008.511.
Yaqub, M., van Berckel, B.N., Schuitemaker, A., Hinz, R., Turkheimer, F.E., Tomasi, G., Lammertsma, A.A., Boellaard, R., 2012. Optimization of supervised cluster analysis for extracting reference tissue input curves in (R)-[11C]PK11195 brain PET studies. J. Cerebr. Blood Flow Metabol. 32 (8), 1600–1608. https://doi.org/10.1038/jcbfm.2012.59.
Yesavage, J.A., Brink, T.L., Rose, T.L., Lum, O., Huang, V., Adey, M., Leirer, V.O., 1983. Development and validation of a geriatric depression screening scale: a preliminary report. J. Psychiatr. Res. 17 (1), 37–49.
Yokokura, M., Mori, N., Yagi, S., Yoshikawa, E., Kikuchi, M., Yoshihara, Y., Wakuda, T., Sugihara, G., Takebayashi, K., Suda, S., Iwata, Y., Ueki, T., Tsuchiya, K.J., Suzuki, K., Nakamura, K., Ouchi, Y., 2011. In vivo changes in microglial activation and amyloid deposits in brain regions with hypometabolism in Alzheimer's disease. Eur. J. Nucl. Med. Mol. Imag. 38 (2), 343–351. https://doi.org/10.1007/s00259-010-1612-0.
Yu, X., Zhang, Y., Cai, Y., Rong, N., Li, R., Shi, R., Wei, M., Jiang, J., Han, Y., 2024. Asymmetrical patterns of β-amyloid deposition and cognitive changes in Alzheimer's disease: the SILCODE study. Cerebr. Cortex 34 (12). https://doi.org/10.1093/cercor/bhae485 bhae485.
Zheng, W., Cui, B., Han, Y., Song, H., Li, K., He, Y., Wang, Z., 2019. Disrupted regional cerebral blood flow, functional activity and connectivity in Alzheimer's disease: a combined ASL perfusion and resting state fMRI study. Front. Neurosci. 13, 738. https://doi.org/10.3389/fnins.2019.00738.